

# Optimal and wavelet-based shock wave detection and estimation<sup>a)</sup>

Brian M. Sadler, Tien Pham, and Laurel C. Sadler  
Army Research Laboratory, Adelphi, Maryland 20783

(Received 15 May 1997; revised 15 April 1998; accepted 27 April 1998)

Detection and estimation of aeroacoustic shock waves generated by supersonic projectiles are considered. The shock wave is an  $N$ -shaped acoustic wave emanating in the form of an acoustic cone trailing the projectile. An optimal detection/estimation scheme is considered based on a parametric signal plus white Gaussian noise model. To gain robustness and reduce complexity, we then focus on gradient estimators for shock wave edge detection, exploiting the very fast shock rise and fall times. The approach is cast in terms of a wavelet transform where the level of smoothing corresponds to scale. A multiscale analysis is described, consisting of multiscale products, to enhance edge detection and estimation. This method is effective and robust with respect to unknown environmental interference that will generally not exhibit singularities as sharp as the  $N$ -wave edges. Experimental results are presented for discriminating  $N$  waves in the presence of vehicle noise. Results are also shown, as a function of miss distance, for gradient-based detection of simulated small projectile shocks inserted into recorded tank noise. © 1998 Acoustical Society of America. [S0001-4966(98)03008-2]

PACS numbers: 43.60.Cg, 43.28.Mw [JLK]

## INTRODUCTION

We consider optimal and gradient-based detection and estimation of aeroacoustic shock waves generated by supersonic projectiles. This problem arises in military, law enforcement, and other cases. It is desired to detect the presence of a bullet or other projectile, and to estimate the parameters of the shock wave. Detection is useful in a variety of scenarios with application in sniper location as well as on vehicles and aircraft. Of particular interest are robust methods that will work at moderate signal-to-noise ratio (SNR) in the presence of platform noise.

The shock wave is an “ $N$ -shaped” wave emanating in the form of an acoustic cone trailing the projectile.<sup>1</sup> The cone angle is given by  $\arcsin(c/v) = \arcsin(1/M)$ , where  $c$  is the velocity of sound in air,  $v$  is the projectile velocity, and  $M = v/c$  is the Mach number. Letting  $\Delta P$  denote the pressure jump at the start of the  $N$  wave, and  $P_0$  denote ambient atmospheric pressure, then<sup>2</sup>

$$\frac{\Delta P}{P_0} = 0.53d \frac{(M^2 - 1)^{1/8}}{x^{3/4}l^{1/4}}, \quad (1)$$

where  $d$  and  $l$  are the projectile diameter and length, respectively, and  $x$  is the perpendicular distance from the projectile trajectory to the sensor (the nearest point of approach or miss distance). Denoting the length of the  $N$  wave as  $L$ , then

$$L = 1.82d \frac{Mx^{1/4}}{(M^2 - 1)^{3/8}l^{1/4}} \approx 1.82d \left( \frac{Mx}{l} \right)^{1/4}. \quad (2)$$

In Eq. (2)  $L = cT$  is the  $N$ -wave length, where  $T$  is the  $N$ -wave time duration observed by a single sensor. An alter-

native form, often used in supersonic aircraft studies, gives the length of the observed shock wave along the ground as  $L' = LM$ , e.g., see Gierke.<sup>3</sup> Although somewhat complex in nature when first formed, the shock wave assumes the  $N$  shape after propagating  $\approx 50$  projectile diameters, so that Eqs. (1) and (2) are approximations that hold for  $x$  sufficiently large.<sup>2</sup> From Eqs. (1) and (2) we see that the primary factors affecting amplitude and length are  $d$  and  $x$  ( $x$  can be relatively large); amplitude and length are otherwise weakly dependent on the projectile's overall shape and velocity. Experiments show reasonably good agreement with Eqs. (1) and (2), e.g., see Bass *et al.*<sup>4</sup> and Stoughton.<sup>5</sup>

Theoretical characterization of the  $N$ -wave rise time is somewhat more problematic. Weak-shock predictions agree qualitatively with measurements, but tend to significantly underestimate rise times.<sup>5</sup> Issues include the shock strength, turbulence effects, and molecular vibrational relaxation.<sup>4,5</sup> Experiments with small caliber shocks consistently show rise times ranging from less than 1  $\mu$ s for small  $x$ , to greater than 100  $\mu$ s for  $x > 100$  m.

The very fast rise and fall of the shock wave edges leads to the observed  $N$ -wave characteristic, and the linear slope between the edges is generally not dependent on the projectile shape at large miss distances.<sup>2</sup> Thus the observed shock wave shape is largely independent of the projectile shape and velocity after a short propagation distance (see also Refs. 6 and 7). This in turn implies that a general purpose detector can be developed that is applicable to a wide variety of projectiles.

Note that the magnitude of the shock decreases with the miss distance as  $x^{-3/4}$ , while the length increases as  $x^{1/4}$ . We assume that the miss distance  $x$  is not known *a priori* and this, coupled with the direct dependence on projectile diameter  $d$ , implies that an observed  $N$ -wave may have been generated by a continuum of different size projectiles at different

<sup>a)</sup>Part of the results in this paper were presented in the 130th meeting of the Acoustical Society of America, St. Louis, MO, November 1995 [J. Acoust. Soc. Am. **98**, 2968(A) (1995)]; and at the Intl. Conf. Acoust., Speech, and Signal Process. (ICASSP-97), Munich, Germany, April 1997 [Proc. Intl. Conf. Acoust. Speech, and Signal Process. Vol. 3, pp. 1889–1992 (1997)].

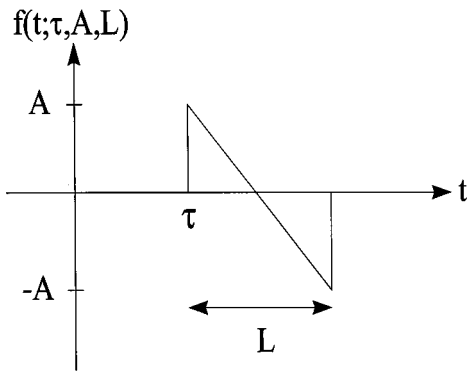


FIG. 1. Ideal parameterized shock wave (or  $N$ -wave)  $f(t)$ .

ranges. For example, one cannot necessarily discriminate between a larger projectile further away versus a smaller projectile that is closer to the sensor. Estimation of  $x$ ,  $v$ , and projectile type from a single sensor are generally not possible without *a priori* knowledge or constraints on the problem. It is possible, however, to estimate these quantities in some scenarios, especially with multiple sensors. An example is a firing range application.<sup>8,9</sup> Here the angle of arrival is known, allowing estimation of the projectile velocity via the change in  $L$  versus time, obtained with multiple sensors along the projectile path. The velocity and length estimates may then be used to classify projectiles. We also note that low precision microphones may be used in practice, reducing system cost but making absolute determination of shock wave pressure unreliable.

The  $N$ -wave can be parameterized in terms of time of arrival  $\tau$ , amplitude  $A$ , and length  $L$ . In the following, for convenience, we use amplitude  $A$  rather than pressure  $\Delta P$ . An idealized constant slope  $N$  wave is shown in Fig. 1 and described by (e.g., see Pierce,<sup>10</sup> Chap. 11)

$$f(t; \theta) = Af\left(\frac{t - \tau}{L}\right), \quad \tau \leq t \leq \tau + L, \quad (3)$$

where

$$f(t) = 1 - 2t, \quad 0 \leq t \leq 1, \quad (4)$$

is the amplitude and length-normalized signal, and  $\theta = [\tau, A, L]$  denotes the parameter vector. Acceptable ranges for  $\theta$  are assumed to be known from context, based on Eqs. (1) and (2).

In the following we discuss two approaches for detecting  $f(t; \theta)$  and estimating  $\tau$ ,  $A$ , and  $L$ . First, we consider the optimal detection-estimation scheme based on a Gaussian noise assumption, leading to a matched filter-type implementation. This approach has high complexity and does not model interference. Next, as an alternative, we consider the use of gradient estimators as a means of detecting the rising and falling edges of the  $N$  wave, an approach that requires sufficient SNR but has much lower complexity and is robust to interference. Smoothed gradient estimators are described in the context of wavelets, and a multiscale analysis is described that exploits multiple levels of smoothing simultaneously. Simulations and experiments with measured  $N$ -waves and vehicular interference sources complete the paper.

## I. OPTIMAL DETECTION AND ESTIMATION IN GAUSSIAN NOISE

In this section we consider optimal Bayes and maximum-likelihood methods for detection of the shock wave and estimation of its parameters. These methods rely on an additive Gaussian noise assumption, leading to a parameterized matched filter-bank approach. However, as often happens under an additive Gaussian noise assumption, the resulting detector is generally not robust to violations of this assumption, such as in the presence of strong interfering acoustic sources.

Consider the binary hypothesis test

$$\begin{aligned} H_1: \quad r(t) &= f(t; \theta) + n(t), \quad 0 \leq t \leq T \gg L, \\ H_0: \quad r(t) &= n(t), \end{aligned} \quad (5)$$

where  $n(t)$  is white Gaussian noise with variance  $N_0$ . We assume that  $f(t; \theta)$  is completely contained in the interval  $T$ . This problem is well studied in the context of radar where  $f(t)$  is typically a narrow-band sinusoidal pulse of possibly unknown time-of-arrival, frequency, and phase; e.g., see Helstrom.<sup>11</sup> If  $\theta$  were known then the optimal decision would be based on the matched filter. The Bayes-optimal decision rule is based on the likelihood ratio

$$\lambda(\mathbf{r}) = \frac{\int_{\theta} p_1(\mathbf{r}|\theta) w_{\theta}(\theta) d\theta}{p_0(\mathbf{r})} \stackrel{H_1}{\geq} \lambda_0, \quad (6)$$

where  $w_{\theta}(\theta)$  is the *a priori* joint probability density of  $\theta$ ,  $p_i(\cdot)$  is the likelihood function under the  $i$ th hypothesis, and  $\mathbf{r}$  is the set of samples of  $r(t)$ ,  $0 \leq t \leq T$ . We further assume that the unknown parameters in  $\theta$  are independent. This last assumption is not strictly true:  $A$  and  $L$  both depend on the same parameters in Eqs. (1) and (2). However, we are assuming the quantities  $d$ ,  $v$ ,  $l$ , and  $x$  are unknown.

Next we consider the form of the optimal detection receiver. We begin by assuming  $L$  is random, and then broaden the analysis to allow  $\tau$  and then  $A$  also to be random. Suppose that  $L$  is random with  $\tau$  and  $A$  known, and assume a uniform prior probability density on  $L$ , so that  $L \sim \mathcal{U}[L_0, L_1]$ , with  $0 < L_0 < L_1$ . Now,

$$\begin{aligned} p_1(\mathbf{r}) &= c_0 \int_{L_0}^{L_1} \exp\left\{ \frac{-1}{N_0} \int_0^T [r(t) \right. \\ &\quad \left. - f(t; L)]^2 dt \right\} \frac{dL}{L_1 - L_0}, \end{aligned} \quad (7)$$

while under  $H_0$

$$p_0(\mathbf{r}) = c_0 \exp\left\{ \frac{-1}{N_0} \int_0^T [n(t)]^2 dt \right\}, \quad (8)$$

with  $c_0$  a constant. Defining the signal energy

$$E_f = \int_0^T [f(t)]^2 dt = \frac{LA^2}{3}, \quad (9)$$

and also defining

$$q(L) = \int_0^T r(t) f(t; L) dt, \quad (10)$$

then we can write the likelihood ratio as

$$\begin{aligned} \lambda(\mathbf{r}) &= \int_L \lambda(\mathbf{r}|L)w(L)dL \\ &= \int_{L_0}^{L_1} \exp\left\{\frac{-E_f}{N_0} + \frac{2A}{N_0} q(L)\right\} \frac{dL}{L_1-L_0}. \end{aligned} \quad (11)$$

For the purposes of implementation we partition the uniform density for  $L$  into a discrete set of equally likely lengths  $L_i$ ,  $i=1,\dots,M$ , so that we may replace the integration of Eq. (11) by the summation

$$\lambda(\mathbf{r}) \approx \frac{1}{M} \sum_{i=1}^M \lambda(\mathbf{r}|L_i). \quad (12)$$

A similar argument for the time of arrival  $\tau$  may be applied, where we take  $\tau \sim \mathcal{U}[0, \tau_1]$ . For  $L$  and  $\tau$  random and assuming  $A$  known, then

$$\begin{aligned} \lambda(\mathbf{r}) &= \int_0^{\tau_1} \lambda(\mathbf{r}|\tau) \frac{d\tau}{\tau_1} \\ &= \int_0^{\tau_1} \int_{L_0}^{L_1} \exp\left\{\frac{-E_f}{N_0} + \frac{2A}{N_0} q(L)\right\} \frac{dL}{L_1-L_0} \frac{d\tau}{\tau_1}, \end{aligned} \quad (13)$$

where  $\lambda(\mathbf{r}|\tau)$  is now given by Eq. (11). Partitioning the delays  $\tau$  into an equally likely set  $\tau_j$ ,  $j=1,\dots,N$ , then

$$\lambda(\mathbf{r}) \approx \frac{1}{MN} \sum_{i=1}^M \sum_{j=1}^N \lambda(\mathbf{r}|L_i, \tau_j), \quad (14)$$

with

$$\lambda(\mathbf{r}|L_i, \tau_j) = \exp\left\{\frac{-E_f}{N_0} + \frac{2A}{N_0} q(L)\right\}. \quad (15)$$

Note that for  $L$  and/or  $A$  random  $E_f=LA^2/3$  is not constant from realization to realization. Thus in the implementation based on Eq. (14) the correction term  $-E_f/N_0$  is applied in each branch for normalization.

Finally, consider the effects of  $A$ ,  $L$ , and  $\tau$  random. Now  $\lambda(\mathbf{r}|A)$  is given by Eq. (13), and we note that  $\lambda(\mathbf{r}|A)$  is maximized for any fixed  $A>0$  if  $q$  is maximized. Note from Eq. (10) that  $q(L)$  is a simple correlation between the model and the received data. Thus a decision may be made by comparing the correlation  $q$  to a threshold, and  $q$  provides a uniformly most powerful (UMP) test with respect to amplitude  $A$ . Note that we are exploiting the fact that  $A>0$ ; if  $A$  is bipolar then no UMP test exists and we must resort to a suboptimal two-sided test.

An alternative to Eq. (14) is the ‘‘maximum-likelihood’’ (ML) detector, which is an approximation to Eq. (14). This detector proceeds by taking the maximum of the  $M$  paths, as shown in Fig. 2, and corresponds to a bank of matched filters matched to the various lengths  $L$  [denoted MF ( $L_i$ ) in the figure]. It arises from the multiple hypothesis test

$$\begin{aligned} H_0: \quad r(t) &= n(t), \quad 0 \leq t \leq T \gg L, \\ H_i: \quad r(t) &= f(t; \theta_i) + n(t) \end{aligned} \quad (16)$$

for  $i=1,\dots,MN$ , where  $\theta_i$  is the  $i$ th parameter vector out of the  $MN$  possible choices. The ML detector also corresponds

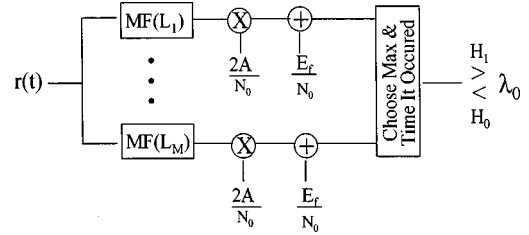


FIG. 2. Maximum-likelihood shock wave detector in white Gaussian noise.

to forming the maximum-likelihood estimates of the parameters and then using these in the likelihood ratio as if they were the true  $\theta$ . Thus the detector of Fig. 2 is appealing for our problem because it simultaneously yields estimates  $\hat{\tau}$  and  $\hat{L}$ . Given  $\hat{\tau}$  and  $\hat{L}$  an optimal estimate of  $A$  is easily obtained via linear regression over  $\hat{\tau} \leq t \leq \hat{L}$ . Because  $E_f$  can change, a normalization is required before applying the common threshold  $\lambda_0$ . Alternatively, the correlation statistic  $q$  in Eq. (10) can be employed requiring a separate threshold for each channel.

Note that the complexity of the scheme in Fig. 2 is proportional to  $M \times N$  [see Eq. (14)]. With fast implementation of the matched filters (via the FFT) the complexity is therefore of order  $O(M \times T \log T)$ , where  $T$  is the data record length [see Eq. (5)]. Thus the search over  $M$  different shock wave lengths creates significant complexity in the detector.

Without knowledge of the prior probabilities of  $H_1$  vs  $H_0$  it is prudent to select the decision threshold  $\lambda_0$  via the Neyman–Pearson criterion so as to maximize the probability of detection for a fixed probability of false alarm. This assumes that  $N_0$  is known or can be estimated. Here,  $H_0$  is a simple hypothesis, so that for  $\tau$  known the probability of false alarm  $P_{fa}$  is given by

$$P_{fa} = \int_{R_1} \rho_0(y) dy = \frac{1}{(2\pi)^{1/2}} \int_{\gamma}^{\infty} e^{-y^2/2} dy, \quad (17)$$

where  $\rho_0(y)$  is the Gaussian pdf of the noise and the last equality assumes unit variance. Given a desired  $P_{fa}$ ,  $\gamma$  may be obtained from Eq. (17). This, together with known or estimated values for  $N_0$  and  $E_f$ , are sufficient to set the detection threshold; for example, see Ref. 12, Sec. 6.2. In the more general case of the ML detector in Fig. 2 with unknown arrival time,  $P_{fa}$  and the probability of detection  $P_{det}$  are more difficult to calculate. When the SNR is large enough to be useful in practice then  $P_{det}$  can be approximated by the detection probability arising as if the arrival time  $\tau$  were known *a priori*.  $P_{fa}$  can be approximated using the rate at which the detection statistic crosses the threshold, e.g., see Ref. 11, Chap. 7.

## II. EDGE DETECTION AND MULTISCALE WAVELET ANALYSIS

In this section we consider gradient-based detection and estimation schemes as an alternative to the optimal Gaussian noise solution of the previous section. This approach exploits the very fast rise and fall times of the shock wave edges. We are motivated by reduced complexity implementation, as

well as the desire to be robust to strong interferers, such as platform noise. With strong unknown interference an optimal solution will generally be unavailable.

### A. Edge detection

Gradient operators are a classical means of estimating step changes in signals and images, and may be applied for detection of shock edges. Commonly used 2-D operators such as Roberts, Prewitt, and Sobel reduce to an FIR filter with impulse response  $[-1,0,1]$  in one dimension (e.g., see Jain<sup>13</sup>). More general extensions, so-called filtered derivative methods, combine smoothing with gradient estimation to reduce noise effects, and are more effective when higher noise levels are encountered. These methods are attractive due to low complexity linear implementation. They also tend to be localized, providing robustness to highly varying backgrounds and multiple change points. Alternative step-change detection methods are based on detecting changes in statistical distributions, such as a step change in the mean, and typically require a moderate to large sample size around a single point of change, e.g., see Basseville and Nikiforov.<sup>14</sup> Thus the latter may be difficult to apply in the present context.

A filtered derivative method that has received a lot of attention is the derivative of Gaussian (dG), which estimates the gradient after smoothing with a Gaussian function. The level of smoothing is determined by the variance of the Gaussian. The dG approach can be derived under criteria of detection and localization (see Canny,<sup>15</sup> Tagare and deFigueiredo,<sup>16</sup> and Koplowitz and Greco<sup>17</sup>). The problem can also be formulated in terms of zero crossings of the second derivative, such as the Laplacian of Gaussian approach which is equivalent to dG in 1-D. Attempting to achieve simultaneous detection and estimation results in a tradeoff between the level of smoothing and the variance of the estimated step location, and this tradeoff is sensitive to the edge shape and SNR. On the one hand, only very local information is required for optimal estimation of the edge location.<sup>18,19</sup> On the other hand, a large data window is desired to detect step changes, in essence allowing sufficient smoothing to estimate signal levels before and after the change. In addition, the optimal smoothing level is not typically known *a priori*.

### B. A wavelet framework

The problems with choosing *a priori* the level of smoothing appropriate for gradient estimation can be overcome to some extent by employing a multiscale analysis, i.e., combining results over multiple levels of smoothing. It is well known that wavelets may be used for detecting and characterizing singularities.<sup>20</sup> This has been applied to edge detection in images via analysis across scale space, putting earlier work of Canny<sup>15</sup> and others into the wavelet transform framework.<sup>21</sup>

Consider a wavelet  $\psi(t)$  that consists of the first derivative of a smoothing function  $u(t)$ , given by  $\psi(t)$

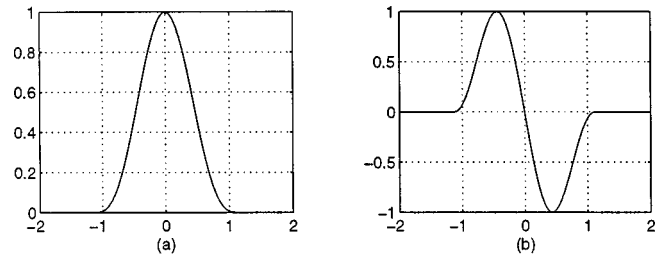


FIG. 3. (a) A cubic spline smoothing function  $u(t)$  that is approximately Gaussian, and (b) its derivative  $\psi(t) = du(t)/dt$ .  $\psi_s(t) = (1/s)\psi(t/s)$  is a wavelet yielding a filter bank that estimates the derivative at a level of smoothing increasing with the scale  $s$ .

$= du(t)/dt$ . With easily achievable constraints on  $\psi(t)$  then, for some function of interest  $g(t)$ , it is straightforward to show that<sup>20</sup>

$$W_s g(t) = g(t) * \left( s \frac{du_s}{dt} \right) (t) = s \frac{d}{dt} (g * u_s)(t), \quad (18)$$

where  $u_s(t) = (1/s)u(t/s)$  and  $*$  denotes convolution. Thus for appropriate choice of  $u(t)$ ,  $W_s g(t)$  can be interpreted as a derivative of a local average of  $g(t)$  where the degree of smoothing depends on  $s$ . The result is estimation of the derivative of  $g(t)$  at various levels of smoothing (scales). In Ref. 21 Mallat and Zhong developed a nonorthogonal DWT based on  $u(t)$  being a cubic spline approximation to a Gaussian, shown in Fig. 3. We refer to this particular DWT as the MZ-DWT (Matlab code for this algorithm is listed in Ref. 22). Thus the MZ-DWT implements the dG algorithm at various smoothing levels. We note that the discretization here is dyadic in scale ( $s = 2^j$ ,  $j \in \mathcal{Z}$ ) but is not dyadic in time (shift), which corresponds to a filter bank with no down sampling. The MZ-DWT of  $g(n)$ ,  $1 \leq n \leq N$ , consists of

$$W_{2^j} g(n), \quad j = 1, 2, \dots, J-1, \quad (19)$$

where  $J = \log_2 N$ , plus the remaining coarse scale information denoted by  $S_J(n)$ . Thus the MZ-DWT, consisting of  $J \times N$  points, is overcomplete (nonorthogonal). This contrasts with the (perhaps more commonly encountered) orthogonal wavelet transforms where the number of coefficients decreases with scale. The inverse DWT may also be readily computed, enabling filtering and reconstruction.

The impulse responses of the MZ-DWT filter bank over several scales are shown in Fig. 4. Some frequency responses are illustrated in Fig. 5; the linear slope region of each filter yields an approximation to differentiation in the various passbands. From now on we use  $W_s g(n) = W_{2^j} g(n)$  to specifically denote the MZ-DWT at scale  $s = 2^j$ ,  $j = 1, 2, \dots$ , and at sampling time  $n$ .

### C. Multiscale analysis

A detection strategy may be based on one or more scales of  $W_s g(n)$ . We emphasize that the lowest scale corresponds to a simple two-point gradient estimator [see Fig. 4(a)]. Various multiscale strategies are possible, e.g., Li *et al.* developed *ad hoc* modifications for the ECG problem.<sup>23</sup>

Consider a multiscale analysis by forming the product

$$p(n) = \prod_{j=j_0}^{j_1} W_{2^j} g(n), \quad (20)$$

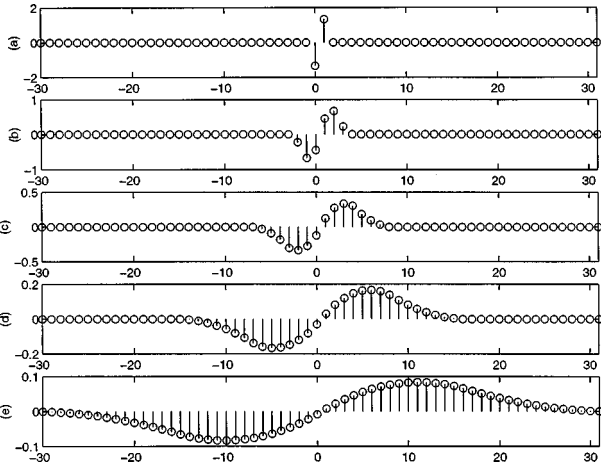


FIG. 4. The impulse responses of Mallat's discrete wavelet transform (MZ-DWT) for the first five scales, panels (a) through (e), respectively. These approximate derivative-of-Gaussian (dG) gradient estimation for various levels of smoothing. Note that (a) corresponds to unsmoothed estimation.

illustrated in Fig. 6. This is a distinctly nonlinear function of the input time series  $g(n)$ . The function  $p(n)$  will show peaks at the  $N$ -wave edges, and will have relatively small values elsewhere. The idea of a cross-scale correlation was developed by Rosenfeld for edge detection in images,<sup>24,25</sup> and recently used in the wavelet framework for signal and image denoising by Xu *et al.*<sup>26</sup> The use of  $p(n)$  for detection exploits the MZ-DWT response to the signal and noise in a beneficial way. Singularities produce cross-scale peaks in  $W_{2^j} g(n)$ , and these are reinforced in  $p(n)$ . Although particular smoothing levels may not be optimal, the nonlinear combination tends to reinforce the peaks while suppressing spurious noise peaks. The signal peaks will align across scale for the first few scales, but not for all scales because increasing the amount of smoothing will spread the response and cause singularities separated in time to interact. Thus choosing  $j_1$  too large will result in misaligned peaks in  $p(n)$ . In practice the choice of  $j_1$  is limited to roughly  $j_1 \leq 5$ ; in our examples we use  $j_0 = 1$  and  $j_1 = 3$ . An odd number of terms in  $p(n)$  preserves the sign of the edge. The complexity of the

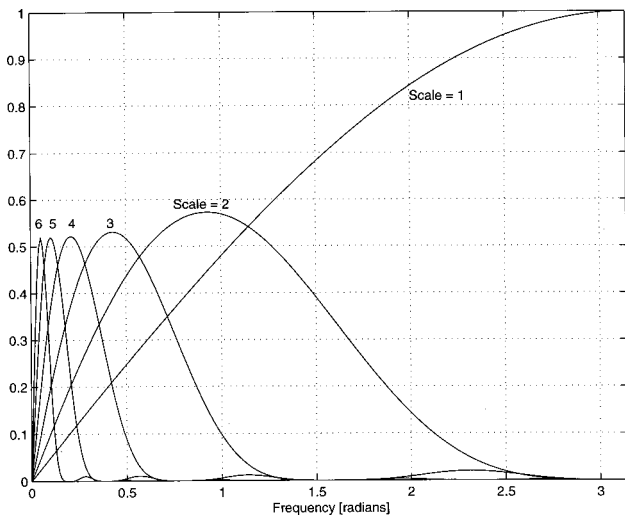


FIG. 5. The frequency response of the MZ-DWT arising from the filters of Fig. 4, shown for the first six scales.

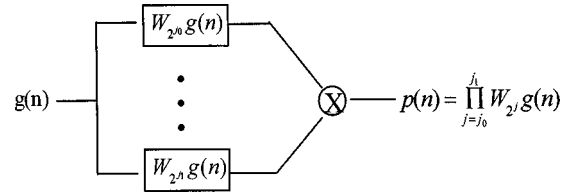


FIG. 6. Computation of  $p(n)$ , the discrete-wavelet transform cross-scale product.

edge detection approach is low. Each scale of  $W_s g(n)$  requires an FIR filter, and formation of  $p(n)$  requires  $j_1 - j_0 + 1$  multiplies per sample, with  $j_1 - j_0 + 1 = 3$  in our examples.

Also motivating use of  $p(n)$  is the MZ-DWT response to white noise across scales. Let  $v(n)$  denote a white noise random process, and  $W_{2^j} v(n)$  its MZ-DWT. It can then be shown that the expected number of maxima of  $W_{2^{j+1}} v(n)$  is one half the expected number of maxima in  $W_{2^j} v(n)$ .<sup>20</sup> Thus due to the increased smoothing at each successive scale, as the scale increases by one the number of maxima decreases by half. The result is that maxima in the cross-scale product  $p(n)$  due to noise are strongly suppressed, while maxima due to the signal are reinforced.

Statistical analysis of  $p(n)$  is given in Ref. 27, with performance analysis for step changes in additive independent Gaussian and non-Gaussian noise. For white noise input to the DWT, we have shown that

$$r_p(m) \triangleq \frac{E[p(n)p(n+m)]}{E[p^2(n)]} \approx \delta(m), \quad (21)$$

for  $j_0 = 1, j_1 - j_0 \geq 2$ , where  $\delta(m)$  is the delta function. Thus  $p(n)$  is a whitened process, despite its nonlinear nature. This is intuitively apparent from study of Fig. 5. The time domain product of the outputs of the DWT filters corresponds to convolution in the frequency domain; convolution of these filter shapes results in a largely flat spectrum for  $p(n)$ . We have also shown that the probability density function of  $p(n)$  is in general heavy tailed non-Gaussian.

## D. Two experimental examples

Figures 7 and 8 illustrate the application of the MZ-DWT to obtain  $p(n)$ . Figure 7(a) shows both an experimentally measured shock wave and a simulated shock wave time series concatenated together. The measured shock wave (the first 200 points) was obtained from a 38-mm-diam projectile (a tank round) at a sampling rate of 48 kHz; this represents a high quality, high SNR measurement. The noise-free simulated shock wave ( $n = 201 - 400$ ) was generated by sampling Eq. (3) to approximately match the measured one, with amplitudes normalized for display. Also shown in Fig. 7(b)–(e) are  $W_{2^j} g(n)$  for the first four scales ( $j = 1, \dots, 4$ ). The increase in smoothing with scale is apparent, and the resulting smoothed derivative estimates show the  $N$ -wave edges clearly. The resulting normalized cross-scale product  $p(n)$  is shown in Fig. 7(f), for  $j_0 = 1$  and  $j_1 = 3$ , depicting clean peaks aligned with the shock wave edges. Note that both the

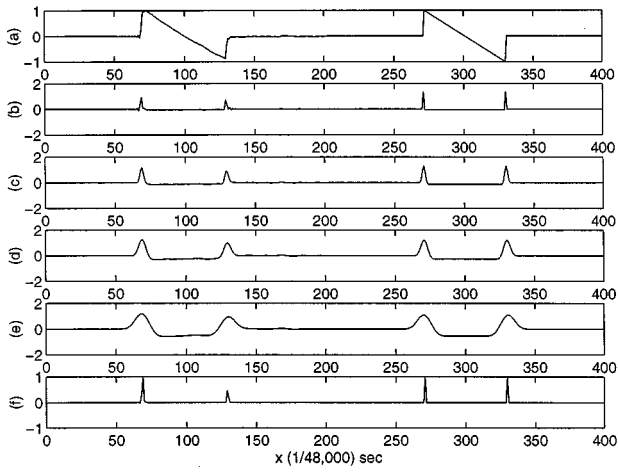


FIG. 7. Measured ( $n=1-200$ ) and simulated ( $n=201-400$ ) shock wave for  $d=38$  mm projectile at 48 kHz sampling rate: (a) time series; (b)–(e) first 4 scales of MZ-DWT; (f) normalized product of first 3 MZ-DWT scales.

leading and trailing edge of the  $N$  wave are positive going, resulting in positive peaks in  $W_{2j} g(n)$ , hence in this application we can reject negative peaks in  $p(n)$ .

Figure 8 depicts similar results based on a recorded shock wave of a 12.7-mm projectile at a 48-kHz sampling rate (note the two echoes following the original shock). This noisy, low SNR recording results in many false peaks in the lower MZ-DWT scales. If one were restricted to a single scale for analysis, this might be the third [Fig. 8(d)]. However,  $p(n)$  taken over the first three scales shows distinct peaks for the initial pulse and the echoes, despite the numerous false peaks in the lower scales of the MZ-DWT.

### E. Estimation and reconstruction

As in the ML detection scheme of Fig. 2, DWT-based detection simultaneously yields estimates  $\hat{\tau}=n_1$  and  $\hat{L}=n_2 - n_1$ , where  $n_1$  and  $n_2$  are the estimated shock edge times. Based on the parametric signal model it remains to estimate  $A$ . Because of the assumed linear slope then, in white Gaussian noise, the optimal estimate of the entire waveform  $f(n)$

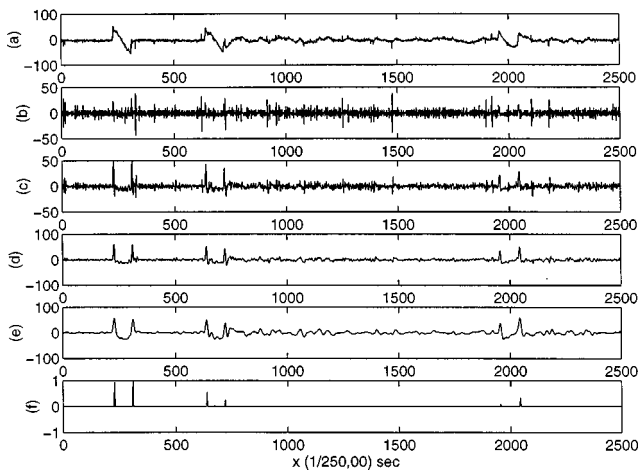


FIG. 8. Measured shockwave for  $d=12.7$  mm projectile at 48 kHz sampling rate: (a) time series; (b)–(e) first 4 scales of DWT; (f) normalized product of first 3 DWT scales.

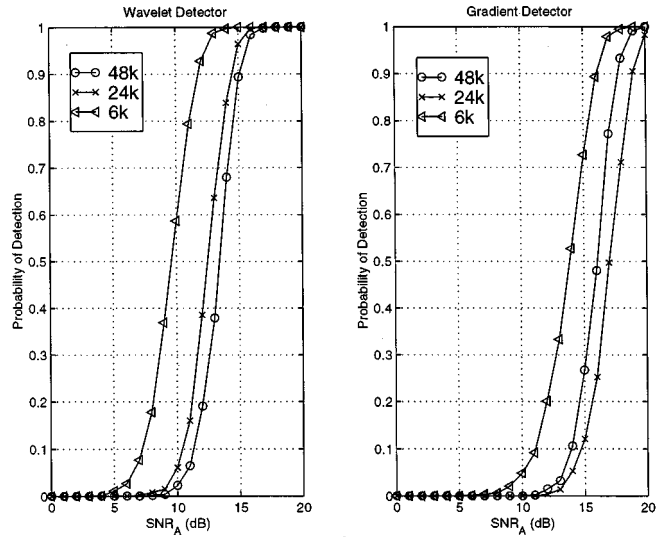


FIG. 9. Detection simulation for a shockwave in additive white Gaussian noise comparing multiscale wavelet-product detection and unsmoothed gradient detection. Here  $\text{SNR}_A$  depends on shock amplitude versus additive white noise variance.

is simply obtained via least-squares line fitting (linear regression) over the noisy observations for  $n \in [n_1, n_2]$ . In practice the  $N$ -wave peaks will not be strictly equal in magnitude; estimates of these  $N$ -wave maxima and minima arise from the endpoints of the linear fit to the data. Another simple estimate of  $A$  is to form  $\hat{A}=0.5[f(n_1)-f(n_2)]$ . The latter estimate may be more appropriate under heavy interference.

Wavelet denoising (i.e., filtering for noise removal via the WT) can be achieved with the DWT employed here.<sup>20,26</sup> These edge-preserving denoising algorithms rely on signal reconstruction from the DWT maxima via alternating projection methods, and do not assume knowledge of the time domain waveform.<sup>21,28</sup>

## III. SIMULATION AND EXPERIMENTAL RESULTS

### A. Shock detection in Gaussian noise

In this example we consider gradient estimation of simulated shock waves in additive white Gaussian noise. Detection results are shown in Fig. 9. The shock wave was constructed using Eq. (3), with length  $L$  established from Eq. (2) using the parameters in Table I, corresponding to a small projectile ( $d=5.56$  mm) at a moderate miss distance (50 m). A sampling rate of 125 000 samples/s was assumed, with  $y(n)=Af(n)+v(n)$ , the ideal shock wave  $f(n)$  plus additive noise  $v(n)$ . Table I values lead to a shock duration of about 36 samples. The signal-to-noise ratio was defined as

$$\text{SNR}_A = 10 \log_{10} \frac{A^2}{\sigma_v^2}, \quad (22)$$

TABLE I. Shock wave simulation parameters for example 1.

$c$ (m/s)	$M$	$d$ (mm)	$l$ (mm)	$x$ (m)
355	2.7	5.56	$3d$	50

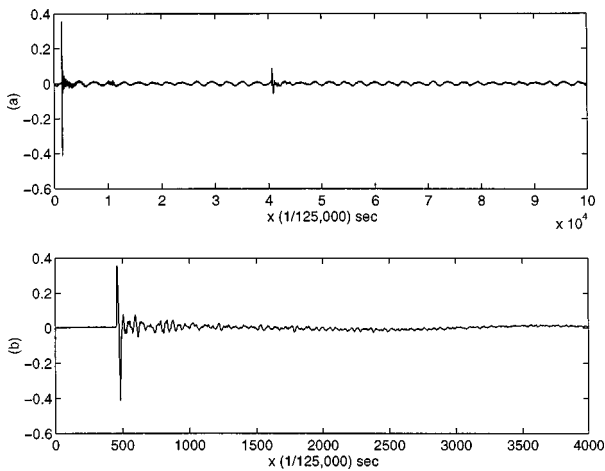


FIG. 10. Measured shock wave for  $d=5.56$  mm projectile at 125 kHz sampling rate in presence of idling vehicle: (a) 0.8 s of time series showing shock (near  $n=0$ ) and muzzle blast (after  $n=40\,000$ ); (b) zoom of time series showing shock wave.

where  $A$  is the shock amplitude and  $\sigma_v^2$  is the noise variance. The definition of  $\text{SNR}_A$  shows the detection performance as a direct function of the amplitude, as opposed to the more standard definition based on the signal energy. The use of  $\text{SNR}_A$  is more appropriate in this case as the detectors rely on the local edge information only, and do not exploit the entire shock waveform.

To simulate rise time and system bandwidth effects, three low-pass filters were designed with bandwidths of 6, 24, and 48 kHz, respectively. Each filter was designed using the Remez exchange algorithm with 50-dB stop-band suppression and a 1-kHz roll-off region, and each had 170 taps. The noisy signal  $y(n)$  was then passed through each filter and detection tests carried out using (i)  $p(n)$  in Eq. (20) with  $j_0=1$  and  $j_1=3$ , and (ii) a simple gradient operator with impulse response  $[-1,0,1]$ . Data records of length  $3 \times 512 = 1536$  were used with the shock wave centered in the record to insure the low-pass filters were in steady state before and after the shock. Detection thresholds were established yielding no false alarms over 100 000 noise training samples. Successful detection was declared if both  $N$ -wave edges were detected above threshold. Results in Fig. 9 are averages over 1000 Monte Carlo trials for each value of  $\text{SNR}_A$ . The results show a 4–5 dB performance gain in using  $p(n)$  over a simple unsmoothed gradient estimator, reflecting the benefits of smoothing at lower  $\text{SNR}_A$ .

## B. Experimental shock detection in platform noise

Next we show results based on experimentally collected data on a noisy platform. Figure 10(a) shows a time series collected from a microphone placed 5 ft off the ground and 3 ft behind a military HMMWV (jeep) with its diesel engine idling. The data were collected with a sampling rate of 125 kHz, such that the time series in Fig. 10(a), which is composed of 100 000 samples, represents 0.8 s elapsed time. A high velocity rifle with projectile diameter  $d=5.56$  mm was fired past the HMMWV at various miss distances. The data shown here correspond to a miss distance  $x$  of approximately 22 m. The shock wave is evident early in Fig. 10(a), and the

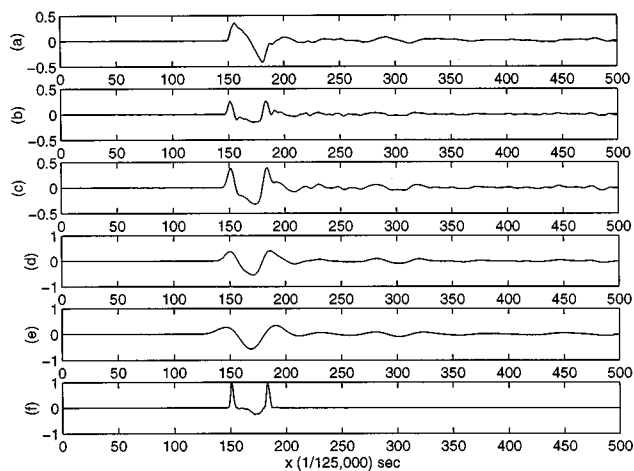


FIG. 11. Zoom of measured shock wave time series from the previous figure: (a) shock wave time series; (b)–(e) first 4 scales of DWT; (f) normalized product of first 3 DWT scales.

muzzle blast follows near the center of the data record. The engine and exhaust sounds are also apparent in the waveform away from the shock and muzzle blast occurrences.

Figure 10(b) is an enlargement of the time series, and the shock wave is now evident. We apply the DWT and form  $p(n)$  via Eq. (20) with  $j_0=1$  and  $j_1=3$ . Results are shown in Fig. 11. Here, Fig. 11(a) is a further enlargement of the time series over 500 samples around the  $N$  wave, (b)–(e) show the first four scales of the MZ-DWT, and (f) shows  $p(n)$  with its peak normalized to unity. Note the sharpening of the peaks in  $p(n)$  versus the unsmoothed gradient estimate [panel (f) versus panel (b), respectively].

We have repeated this experiment with both larger projectiles and smaller miss distances, hence the data shown are the worst case (i.e., smallest amplitude) within the confines of our parameters for this experiment. The engine noise is relatively low pass in comparison to the fast rise time of the  $N$  wave, such that the engine noise does not generally produce significant peaks in  $p(n)$ . Also, the exhaust noise, while of higher bandwidth than the engine sound, is of sufficiently less amplitude than the shock wave in this scenario and hence does not seriously restrict the detection process.

## C. Simulated shock in experimentally collected platform noise

In this example we insert simulated shockwaves into experimentally recorded sound from a moving tank to obtain detection performance as a function of miss distance. Detection results are shown in Fig. 12. An overview of the proce-

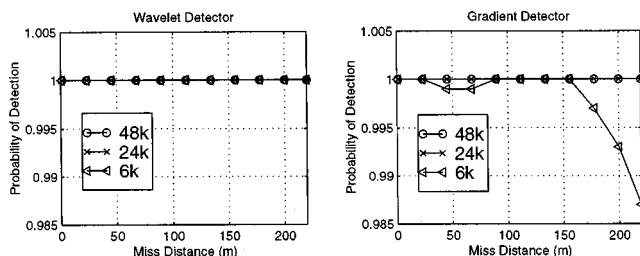


FIG. 12. Detection of simulated  $N$ -wave in recorded tank noise.

TABLE II. Overview of example 3.

1	Shock wave simulation (using parameters from Table III): Find $L$ from Eq. (2). Find shock SPL by linearly interpolating data from Table IV. Find rise-time by interpolating experimental data from Ref. 5, Fig. 6. Filter ideal shock to simulate rise time, yielding $s(n)$ .
2	Form $y(n) = s(n) + x(n) + v(n)$ . Randomly select tank sound segment $x(n)$ from 1.6 s recording. Add white Gaussian noise $v(n)$ at 20 dB ( $10 \log_{10} P_x/P_v $ ).
3	Simulate system bandwidth for three cases: Pass $y(n)$ through low-pass filters with cutoffs of 48, 24, and 6 kHz.
4	Monte Carlo trials: Repeat steps 1–3, 1000 trials for each miss distance and each LPF. Two different detectors compared in Fig. 12.

ture used for this experiment is given in Table II, with parameters given in Table III.

The time series is given by

$$y(n) = s(n) + x(n) + v(n), \quad (23)$$

where  $s(n)$  is a simulated shock,  $x(n)$  is recorded tank sound, and  $v(n)$  is white Gaussian noise. The recording was made with a sampling rate of 125 kHz by driving a tank past a fixed microphone. For this experiment the recording was composed of 200 000 samples (1.6 s) taken when the tank was within roughly one meter of the sensor. The tank SPL was measured by taking the worst case peak-to-peak (p-p) amplitude; for the time series in this experiment this p-p SPL was 132 dB. Each realization of  $y(n)$  was formed by adding  $s(n)$  and  $v(n)$  to the tank recording with the time-of-arrival  $\tau$  randomly selected within the 200 000 samples, and detection results averaged over 1000 Monte Carlo trials for each miss distance. Each realization was of length 1536 samples, with the shock centered in the record. This length was used to insure the low-pass filters described below (and example 1 above) reached steady state response. Additive white Gaussian noise  $v(n)$  was included to further simulate sensor and other noise. The noise  $v(n)$  was added at a fixed power ratio of 20 dB, given by  $10 \log_{10}|P_x/P_v|$ , where  $P_x$  is the average power in the 1.6 s of recorded tank sound and  $P_v$  is the Gaussian noise power.

The shock was simulated as follows. The projectile diameter  $d = 5.56$  mm, length  $l$ , Mach number  $M$ , and the speed of sound in air  $c$ , are given in Table III. The shock duration was obtained via Eq. (2), and rounded to the nearest sample time, with sampling rate matching the recorded tank data at 125 000 samples per second. The shock amplitude was obtained from a linearly interpolated curve based on experimentally collected shock pressure levels. The SPLs are shown in Table IV, obtained by averaging over several shots for each miss distance. These were representative measurements over several trials with different (separately cali-

TABLE III. Shock wave parameters in example 3.

$c$ (m/s)	$M$	$d$ (mm)	$l$ (mm)	$x$ (m)	Samples/s
355	2.7	5.56	$3d$	$1 \leq x \leq 220$	125 000

TABLE IV. Average measured peak-to-peak sound pressure levels for  $d = 5.56$  mm diameter projectile shock waves.

Miss distance (m)	1	7	22
SPL (dB)	150	142	134

brated) microphones. The measurements were conducted in a benign outdoor environment with minimal acoustic interference. The miss distances  $x$  in Table IV are approximate within the experimental error of a marksman firing past a designated point from a range of roughly 200 m. SPLs for arbitrary miss distances in the range  $1 \leq x \leq 220$  m were obtained by interpolating a linear least-squares fit to the data in Table IV, while enforcing a slope proportional to  $x^{-3/4}$  as required by Eq. (1). An ideal shock was then simulated via Eq. (3), where the amplitude was determined with reference to the calibrated shock SPL and the duration in samples determined as described above.

The ideal shock was then filtered to simulate the rise time. The appropriate rise time was obtained by piecewise interpolating the experimental measurements for a 5.56-mm projectile provided by Stoughton (see Fig. 6 of Ref. 5). Experimental results were incorporated due to the lack of a sufficiently accurate theoretical rise time prediction. Rise times for this case varied from less than  $1 \mu\text{s}$  at  $x = 1$  m miss distance to greater than  $40 \mu\text{s}$  at  $x = 220$  m. The ideal simulated shock was then passed through a smoothing filter whose coefficients were all equal to one, with filter extent equal to twice the estimated rise time (quantized to the sampling rate). For example, at  $x = 200$  m the rise time is  $40 \mu\text{s}$ , corresponding to five samples at the sampling rate of  $8 \mu\text{s}$  per sample. So, the ideal shock was smoothed with an FIR filter of length  $2 \times 5 = 10$  with all the filter weights equal to one. This approach to simulating the rise time is conservative in that it overly smooths the shock and results in rise times slower than those observed experimentally.

Each realization of  $y(n)$  was passed through one of three low-pass filters, as in example 1 above, simulating various system bandwidths. Detection results in Fig. 12 are shown for an unsmoothed gradient with impulse response  $[-1, 0, 1]$ , as well as for the wavelet product detector  $p(n)$ , with  $j_0 = 1$  and  $j_1 = 3$  in Eq. (20). Detection thresholds were set to yield no false alarms over a 200 000 sample training set consisting of  $x(n) + v(n)$  for one realization of  $v(n)$ . Detection was declared only if both the leading and trailing  $N$ -wave edges were detected.

Detection results in Fig. 12 predict nearly perfect detection using gradient estimation, out to a miss distance of 220 m. Note that, for a system bandwidth of 6 kHz, the unsmoothed gradient begins to show a loss of performance beyond 150 m. The reduced gradient response is brought on by excessive smoothing. This effect is not evident in the wavelet-product detector, which is able to maintain detection even at the lower system bandwidth of 6 kHz. Thus a higher system bandwidth may be employed that better preserves the rise time, which in turn enables a lower complexity detector. Conversely, a lower system bandwidth may be used with a somewhat more complex detector.

This experiment is intended to be conservative with respect to rise time and the level of additive Gaussian noise. We note, however, that the tank sounds were recorded from a microphone not on the moving platform. Placing the sensor on the tank might lead to somewhat higher noise levels due to vibration, wind, or other effects. The simple gradient-based approach to shock detection appears functional and robust to platform noise due to the fast rise time and relatively large shock amplitude. We also note that larger projectiles will produce louder shocks with faster rise times, hence the detection results will improve in such cases.

#### IV. DISCUSSION

Based on our experimental and simulation results, gradient estimation appears to be a viable low complexity method for detection and estimation of shocks on noisy platforms. Our ability to simulate realistic shocks is limited by the inability to accurately predict rise time. So, the last example of the previous section was intentionally conservative, utilizing a small projectile, a very noisy platform, and significant additive white noise. A larger projectile or quieter platform will improve detectability. While it is important to preserve the rise time to enable accurate edge detection, our results indicate that the relatively loud shock waves can be detected with system bandwidths that are readily achievable.

In its simplest form, gradient estimation can be accomplished with very low complexity. The multiscale wavelet approach provides a technique that incorporates smoothing in the gradient estimation process, without knowing *a priori* what the optimal smoothing level may be. The addition of smoothing provides increased protection against additive noise. The wavelet approach is computationally simple and straightforward to implement in real time applications.

Gradient-based performance depends on the fast rise time and amplitude of the shock edges. This is in contrast to optimal matched filter performance which is theoretically insensitive to the signal shape in additive white Gaussian noise, provided the signal shape is known precisely. Thus in Gaussian noise, the matched filter will generally outperform any other scheme. However, the signal form is only parametrically known, so that a search of the parameter space is necessary, resulting in higher complexity. And, additive interference will quickly degrade the matched filter performance.

The gradient-based approach might be used as a front end to other system layers. In particular the important problem of angle of arrival estimation, requiring multiple sensors, will typically require accurate detection and time-of-arrival estimation at each sensor.

<sup>1</sup>G. B. Whitham, "Flow patterns of a supersonic projectile," *Commun. Pure Appl. Math.* **5**, (1952).

<sup>2</sup>G. B. Whitham, "The behaviour of supersonic flow past a body of revolution, far from the axis," *Proc. R. Soc. London, Ser. A* **201**, 89–109 (1950).

<sup>3</sup>H. von Gierke, "Aircraft noise sources," in *Handbook of Noise Control*, edited by C. Harris (McGraw-Hill, New York, 1957), Chap. 33.

<sup>4</sup>H. E. Bass, B. A. Layton, L. N. Bolen, and R. Raspet, "Propagation of medium strength shock waves through the atmosphere," *J. Acoust. Soc. Am.* **82**, 306–310 (1987).

<sup>5</sup>R. Stoughton, "Measurements of small-caliber ballistic shock waves in air," *J. Acoust. Soc. Am.* **102**, 781–787 (1997).

<sup>6</sup>J. Dumond, E. Cohen, W. Panofsky, and E. Deeds, "A determination of the wave forms and laws of propagation and dissipation of ballistic shock waves," *J. Acoust. Soc. Am.* **18**, 97–118 (1946).

<sup>7</sup>K. Friedrichs, "Formation and decay of shock waves," *Commun. Pure Appl. Math.* **1**, 211–245 (1948).

<sup>8</sup>R. Loucks, B. Davis, L. Moss, T. Pham, and M. Fong, "A method of identifying supersonic projectiles using acoustic signatures," Army Research Laboratory Technical Report, ARL-TR-859, September 1995.

<sup>9</sup>T. Pham, M. Fong, J. Gerber, and K. Tran, "Brassboard design for round discrimination system," Army Research Laboratory Technical Report, ARL-TR-332, February 1994.

<sup>10</sup>A. D. Pierce, *Acoustics, An Introduction to Its Physical Principles and Applications* (McGraw-Hill, New York, 1981).

<sup>11</sup>C. Helstrom, *Elements of Signal Detection and Estimation* (Prentice-Hall, Englewood Cliffs, NJ, 1995).

<sup>12</sup>C. Weber, *Elements of Detection and Signal Design* (Springer-Verlag, New York, 1987).

<sup>13</sup>A. K. Jain, *Fundamentals of Digital Image Processing* (Prentice-Hall, Englewood Cliffs, NJ, 1989).

<sup>14</sup>M. Basseville and I. V. Nikiforov, *Detection of Abrupt Changes, Theory and Application* (Prentice-Hall, Englewood Cliffs, NJ, 1993).

<sup>15</sup>J. Canny, "A computational approach to edge detection," *IEEE Trans. Pattern. Anal. Mach. Intell.* **PAMI-8**, 679–698 (1986).

<sup>16</sup>H. D. Tagare and R. J. P. deFigueiredo, "On the localization performance measure and optimal edge detection," *IEEE Trans. Pattern. Anal. Mach. Intell.* **12**, 1186–1190 (1990).

<sup>17</sup>J. Koplowitz and V. Greco, "On the edge location error for local maximum and zero-crossing edge detectors," *IEEE Trans. Pattern. Anal. Mach. Intell.* **16**, 1207–1212 (1994).

<sup>18</sup>R. Kakarala and A. O. Hero, "On achievable accuracy in edge localization," *IEEE Trans. Pattern. Anal. Mach. Intell.* **14**, 777–781 (1992).

<sup>19</sup>A. M. Reza and M. Doroodchi, "Cramer-Rao lower bound on locations of sudden changes in a steplike signal," *IEEE Trans. Signal Process.* **44**, 2551–2556 (1996).

<sup>20</sup>S. Mallat and W. L. Hwang, "Singularity detection and processing with wavelets," *IEEE Trans. Inf. Theory* **38**, 617–643 (1992).

<sup>21</sup>S. Mallat and S. Zhong, "Characterization of signals from multiscale edges," *IEEE Trans. Pattern. Anal. Mach. Intell.* **14**, 710–732 (1992).

<sup>22</sup>B. M. Sadler and A. Swami, "Analysis of wavelet transform multiscale products for step detection and estimation," Army Research Laboratory Technical Report, to appear 1998.

<sup>23</sup>C. Li, C. Zheng, and C. Tai, "Detection of ECG characteristic points using wavelet transforms," *IEEE Trans. Biomed. Eng.* **42**, 21–28 (1995).

<sup>24</sup>A. Rosenfeld, "A nonlinear edge detection technique," *IEEE Proc.* **58**(5), 814–816 (1970).

<sup>25</sup>A. Rosenfeld and M. Thurston, "Edge and curve detection for visual scene analysis," *IEEE Trans. Comput.* **20**, 562–569 (1971).

<sup>26</sup>Y. Xu, J. Weaver, D. Healy, and J. Lu, "Wavelet transform domain filters: A spatially selective noise filtration technique," *IEEE Trans. Image Process.* **3**, 747–758 (1994).

<sup>27</sup>B. M. Sadler and A. Swami, "On multiscale wavelet analysis for step estimation," *Proc. Intl. Conf. Acoust., Speech, and Sig. Process (ICASSP98)*, to appear; also "On multiscale products for step detection and estimation," *IEEE Trans. Info. Theory*, submitted 1998.

<sup>28</sup>Z. Cvetkovic and M. Vetterli, "Discrete-time wavelet extreme representation: Design and consistent reconstruction," *IEEE Trans. Signal Process.* **43**, 681–693 (1995).